



HAL
open science

Dynamical Response of Solar Wind Charge Exchange Soft X-Ray Emission in Earth's Magnetosphere to the Solar Wind Proton Flux

Yingjie Zhang, Tianran Sun, Jennifer A Carter, Steve Sembay, Dimitra Koutroumpa, Ji Li, Wenhao Liu, Chi Wang

► **To cite this version:**

Yingjie Zhang, Tianran Sun, Jennifer A Carter, Steve Sembay, Dimitra Koutroumpa, et al.. Dynamical Response of Solar Wind Charge Exchange Soft X-Ray Emission in Earth's Magnetosphere to the Solar Wind Proton Flux. *The Astrophysical Journal*, 2023, 948, pp.69. 10.3847/1538-4357/acc326 . insu-04091450

HAL Id: insu-04091450

<https://insu.hal.science/insu-04091450>

Submitted on 8 May 2023

HAL is a multi-disciplinary open access archive for the deposit and dissemination of scientific research documents, whether they are published or not. The documents may come from teaching and research institutions in France or abroad, or from public or private research centers.

L'archive ouverte pluridisciplinaire **HAL**, est destinée au dépôt et à la diffusion de documents scientifiques de niveau recherche, publiés ou non, émanant des établissements d'enseignement et de recherche français ou étrangers, des laboratoires publics ou privés.



Distributed under a Creative Commons Attribution 4.0 International License



Dynamical Response of Solar Wind Charge Exchange Soft X-Ray Emission in Earth's Magnetosphere to the Solar Wind Proton Flux

Yingjie Zhang^{1,2} , Tianran Sun¹ , Jennifer A. Carter³ , Steve Sembay³ , Dimitra Koutroumpa⁴ , Li Ji⁵ ,
Wenhao Liu⁵ , and Chi Wang^{1,2}

¹ State Key Laboratory of Space Weather, National Space Science Center, Chinese Academy of Sciences, Beijing 100190, People's Republic of China; trsun@swl.ac.cn, cw@swl.ac.cn

² College of Earth and Planetary Sciences, The University of Chinese Academy of Sciences, Beijing 101408, People's Republic of China

³ School of Physics and Astronomy, The University of Leicester, Leicester, UK

⁴ LATMOS/IPSL, CNRS, UVSQ Université Paris-Saclay, Sorbonne Université, Guyancourt, France

⁵ Purple Mountain Observatory, Chinese Academy of Sciences, Nanjing, Jiangsu 210023, People's Republic of China

Received 2022 September 11; revised 2023 March 8; accepted 2023 March 8; published 2023 May 8

Abstract

This work studies the dynamic response of solar wind charge exchange (SWCX) soft X-ray emission in the Earth's magnetosphere to the solar wind proton flux. Unlike previous studies that attempted to use complex magnetohydrodynamic models to match the details of observed SWCX of a necessarily limited number of cases, this work focuses on determining the changes over individual observations in a much larger sample. To provide the cleanest test, we selected XMM-Newton observations when the solar wind proton flux changed suddenly by a factor greater than 1.5 and calculated the correlation coefficient between the SWCX emission in the 0.5–0.7 keV band and the proton flux. We find that the dynamical response is weak when the solar wind proton flux is low ($<10,000 \text{ n}^* \text{ km/cc/s}$) because its variation is smaller than the uncertainty due to other emission components, but this response increases with the proton flux and its change value. The response is improved when the valence state of solar wind ions is high, as a higher abundance of ions generating SWCX can produce a greater correlation even though the proton flux is relatively low. It is conducive to the study of interplanetary coronal mass ejections (ICMEs) because ions in ICMEs are usually highly ionized. For XMM-Newton, the 0.5–0.7 keV band shows the strongest correlation, as the instrumental response decreases at lower energies and the SWCX emission decreases at higher energies. Moreover, the closer the satellite line of sight is to the subsolar magnetopause with the strongest SWCX emissivity, the better the correlation.

Unified Astronomy Thesaurus concepts: X-ray astronomy (1810); Diffuse x-ray background (384); Solar coronal mass ejections (310); Solar wind (1534); Solar-terrestrial interactions (1473)

1. Introduction

Solar wind charge exchange (SWCX) occurs when a solar wind high-valence ion interacts with a neutral atom to gain an electron and goes into an excited state. Then the ion returns to its ground state by emitting single or multiple extreme ultraviolet or soft X-ray photons (Cravens 1997).

Emissions from SWCX are typical in the solar system and have been observed on comets (Lisse et al. 1996), Earth (Wargelin et al. 2004), Jupiter (Branduardi-Raymont et al. 2004), Mars (Dennerl et al. 2006), and the Moon (Collier et al. 2014). Soft X-rays emitted by SWCX has been a contaminating foreground in astrophysical observations (see the review of Kuntz 2018); however, it has recently been applied to a developed method for studying the Earth's magnetosphere using panoramic soft X-ray imaging (Branduardi-Raymont et al. 2012; Collier et al. 2012; Sibeck et al. 2018). The Solar Wind Magnetospheric Ionosphere Link Explorer, an ESA–CAS joint soft X-ray imager with a uniquely large field of view (FOV; $16^\circ \times 27^\circ$), will be launched in the future (2024–2025; Branduardi-Raymont et al. 2018; Wang & Branduardi-Raymont 2020).

The SWCX emission intensity of the Earth's magnetosphere along a particular line of sight (LOS) is estimated as (Cravens 2000; Sun et al. 2015, 2019, 2021)

$$I = \frac{1}{4\pi} \int \alpha n_{\text{H}} n_{\text{sw}} v_{\text{rel}} dr \text{ (keV cm}^{-2} \text{ s}^{-1} \text{ sr}^{-1}), \quad (1)$$

where n_{H} is the neutral hydrogen density, n_{sw} is the solar wind proton density, and v_{rel} is the relative velocity, calculated from the solar wind velocity v_{sw} and the thermal velocity v_{th} as $v_{\text{rel}} = \sqrt{v_{\text{sw}}^2 + v_{\text{th}}^2}$. Here α is the total efficiency factor of SWCX, determined as follows:

$$\alpha = \sum_{Xqj} \alpha_{Xqj} = \sum_{Xqj} \sigma_{Xqj} \left[\frac{X^{q+}}{\text{O}} \right] \left[\frac{\text{O}}{n_{\text{sw}}} \right] \text{ (eV cm}^2), \quad (2)$$

where α_{Xqj} is the efficiency factor for a specific transition j from the solar wind ion species (X) in a charge state q that interacts with the neutral hydrogen, σ_{Xqj} is the charge exchange cross section, $\left[\frac{X^{q+}}{\text{O}} \right]$ is the ratio of a specific ion to oxygen ions, and $\left[\frac{\text{O}}{n_{\text{sw}}} \right]$ is the ratio of oxygen ions to solar wind protons.

According to Equations (1) and (2), the important quantities that determine the intensity of magnetospheric SWCX emission are the solar wind proton density and speed, the solar wind ion abundance, the structure of the magnetosheath along the LOS, and the neutral density along the LOS. Of these, the change of

neutral density is likely small over the course of an observation and thus can be ignored, while the solar wind, as well as the structure of the magnetosphere, which is strongly correlated with the solar wind flux, can change substantially over the course of an observation. Therefore, this paper mainly studies the correlation between the magnetospheric SWCX emission and the solar wind proton flux.

Many previous works have conducted observational studies of the correlation between the magnetospheric SWCX emission intensity and the solar wind proton flux. In the case studies, this correlation was sometimes good and sometimes bad (Snowden et al. 2004; Fujimoto et al. 2007; Carter et al. 2010; Ezo et al. 2010, 2011; Ishikawa et al. 2013; Ishi et al. 2019; Asakura et al. 2021; Ishi et al. 2022; Zhang et al. 2022). In statistical studies, such a correlation was often weak or even nonexistent (Snowden et al. 1997; Carter & Sembay 2008; Kuntz & Snowden 2008; Henley & Shelton 2010; Carter et al. 2011, 2012; Henley & Shelton 2012; Kuntz et al. 2015; Whittaker et al. 2016). In fact, the bulk of the above studies not only were based on the observed X-ray data but also compared the observations with SWCX/neutral models of varying degrees of sophistication. Kuntz & Snowden (2008), Carter et al. (2011), Ishikawa et al. (2013), and Ishi et al. (2019) used a very simple model of the magnetosheath coupled to solar wind proton data and a simple neutral density model. Kuntz et al. (2015) and Whittaker et al. (2016) used the magnetohydrodynamic (MHD) model based on solar wind data; the former considered the exospheric and heliospheric neutral distribution, and the latter incorporated the solar wind ion data. Since the detailed MHD simulations require a great deal of time, they must be limited to a relatively small number of cases and thus produce small statistical samples. The less sophisticated models of the magnetosphere can be applied to much larger statistical samples but have typically ignored the ion data. Further, the larger studies have typically been done on an observation-by-observation basis, rather than looking at the changes over individual observations, which obscures the types of changes that would most clearly demonstrate the action of SWCX. Thus, the statistical results of the larger samples are less than satisfactory. Another problem with all of these studies is that they have typically attempted to compare modeled SWCX intensities to observed SWCX intensities, which obscures the dependence on the solar wind flux if there are systematic problems with the models. The systematic problem with the models is the location of the magnetopause. Since the FOV of XMM-Newton is very small, the observed magnetosheath is relatively narrow, so an error in the relative locations of the LOS and magnetopause can not only significantly change the observed X-ray flux but also easily introduce anticorrelations when correlations are expected. Thus, studies that attempt to model the intensity along the LOS can easily miss real correlations between the SWCX emission and the solar wind flux.

This study considers only the dynamical response of the magnetospheric SWCX emission to the solar wind proton flux over the course of individual XMM-Newton observations. Thus, this study is not sensitive to errors in the model of the neutral density. Its sensitivity to the relative location of the LOS and the magnetopause will also be significantly reduced. To produce the cleanest study of the correlation, we consider only observations with strong, sudden changes in the solar wind proton flux. This method leaves only the ion abundance variation to confuse the correlation, and that is dealt with separately. Section 2 describes the method. Section 3 shows the

results. Sections 4 and 5 provide discussions and conclusions, respectively.

2. Method

2.1. Selection Criteria

This paper uses the 30 minute averaged solar wind proton flux from OMNI 1 minute data⁶ and defines the sudden change in solar wind proton flux as (1) the ratio of high flux to low flux, ≥ 1.5 , and (2) the duration of high flux, ≥ 1 hr. This can not only amplify the contribution of the solar wind proton flux change but also make the solar wind proton flux change fall at the boundary between the two bins, which is conducive to highlighting the effect of solar wind proton flux. In this paper, the sudden increase and decrease in the solar wind proton flux are labeled “up” and “down,” respectively.

The European Photon Imaging Camera on the astronomical X-ray satellite XMM-Newton consists of three CCD cameras: MOS1, MOS2 and pn. The selection criteria for XMM-Newton observations during the sudden change in the solar wind proton flux were as follows: (1) available (not contaminated by soft proton flares) time was ≥ 1 hr before and after the sudden change; (2) all three cameras were in full-frame mode, where the extended full-frame mode of the pn was excluded to make the analysis software simpler; and (3) mosaic, windowed, and timing observations were excluded.

Since the near-Earth SWCX emission arises mostly from the magnetosheath, the region between the magnetopause and the bow shock, there was only one condition for selecting XMM-Newton observations affected by SWCX emission: the LOS of XMM-Newton passed through the dayside magnetosheath. The first data set was the position and observation direction of XMM-Newton. The second set was the OMNI 1 minute solar wind data required for the empirical magnetopause model (Shue et al. 1997) and bow shock model (Chao et al. 2002). Figure 1 shows the LOS of an XMM-Newton observation affected by magnetospheric SWCX emission before and after the sudden increase of the solar wind proton flux. It is obvious that the SWCX emissivity increases significantly with the solar wind flux.

According to the above selection criteria, from 2000 January 1 to 2021 January 1, we finally selected 100 cases from XMM-Newton observations. As shown in Figure 2, the selected cases only account for 0.71% of the total XMM-Newton observations, which is reasonable because the soft X-ray signal in Earth space is not the observation target of XMM-Newton. In addition, the time span of the selected cases reached 20 yr, covering almost two solar activity cycles. It is beneficial for our research because it weakens the influence of the annual variation of solar activity on the statistical results.

2.2. Analyzing XMM-Newton Data to Obtain the Count Rate

The Science Analysis System (SAS) software (version 20.0.0) and the current calibration files released on 2021 September 20 were used for the XMM-Newton data analysis. In this paper, the count rate of the 0.5–0.7 keV band is used to characterize the intensity of SWCX emission. This energy band is dominated by the emission lines from O⁶⁺ (O VII) and O⁷⁺ (O VIII), with high intensity and a simple spectrum. In addition, the count rate of the 2.5–5.0 keV band is used to characterize the intensity of other background components. The comparison

⁶ <https://cdaweb.gsfc.nasa.gov/index.html>

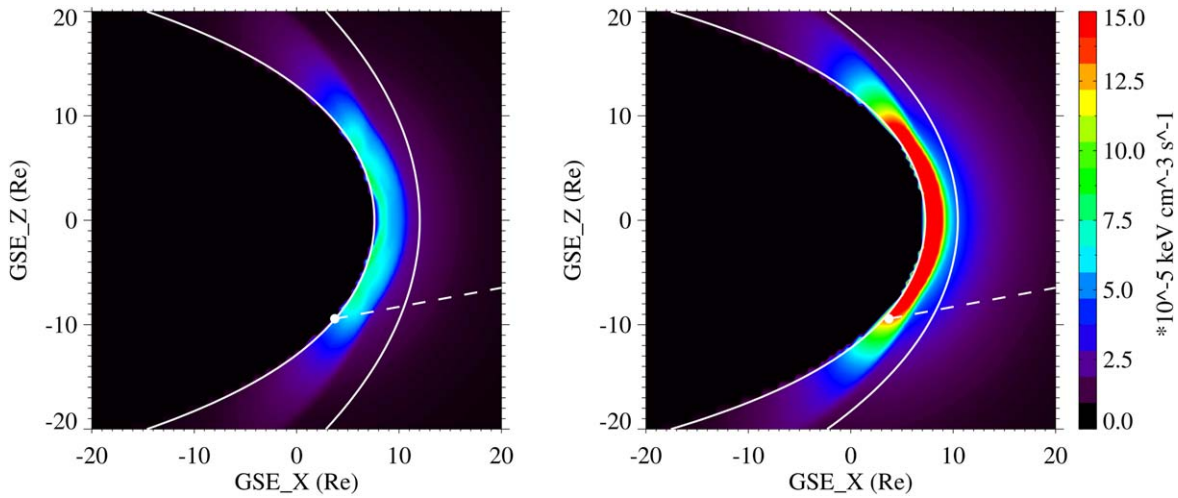


Figure 1. The LOS of an XMM-Newton observation (ID: 0761920901) affected by magnetospheric SWCX emission before (left) and after (right) the sudden increase of the solar wind proton flux in GSE coordinates. The white dot and the dashed line extending from it indicate the position and observation direction of XMM-Newton. The white solid curves show the locations of the magnetopause and bow shock calculated using the average solar wind conditions. Different colors represent the SWCX emissivity simulated by MHD (Sun et al. 2015, 2019, 2021).

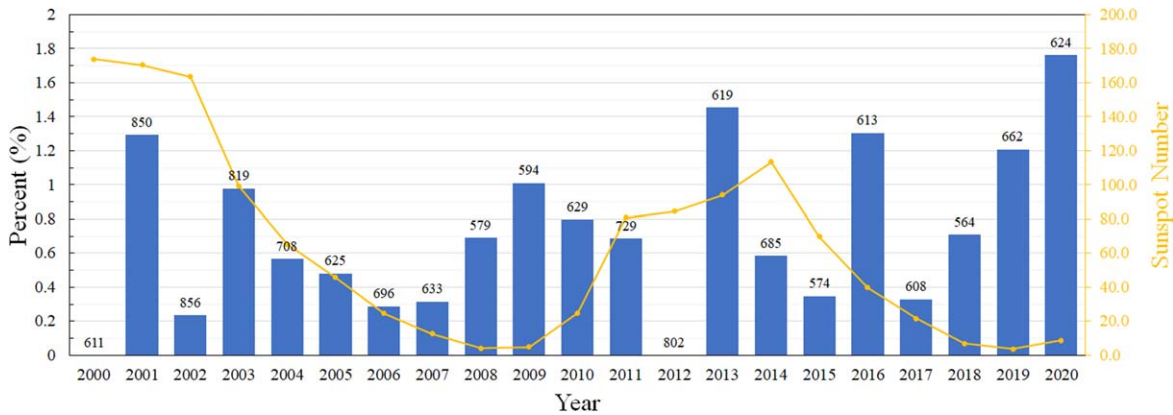


Figure 2. The numbers are the total number of observations taken in that year. The histogram shows the percentage of selected cases in the total observations of that year. The orange line represents the number of sunspots in that year.

of variation in the soft (0.5–0.7 keV) and hard (2.5–5.0 keV) energy bands demonstrates that this change really comes from the SWCX emission (Carter & Sembay 2008).

First, we reprocessed the original data files⁷ by running the SAS tasks emproc for MOS and epproc for pn to obtain the calibrated and concatenated event lists. Second, we selected X-ray events using the following filter expressions: $(PATTERN \leq 12) \& \& (\#XMMEA_EM)$ for MOS and $(PATTERN == 0) \& \& (FLAG == 0)$ for pn. This filter removed events from bright pixels or near CCD boundaries and optimized the energy resolution of pn in the energy range of interest (< 2 keV). Since some individual CCDs in the MOS occasionally operated in anomalous states with a strongly enhanced background at low energy (< 1 keV), we used the SAS task emtaglnoise to examine and exclude those CCDs. Since the SWCX emission was spread over the entire FOV, it was necessary to handle so-called out-of-time (OoT) events in the pn, which were assigned incorrect RAWY values and led to incorrect energy corrections. We created a simulated OoT event list using the SAS task ephchain. We then subtracted the products extracted from this OoT event list from those

extracted from the original event list. Finally, we selected X-ray events within a circular region with a radius of $11'7$ centered on the common sky position of the three cameras.

After the previous steps, the extracted X-ray signal was composed of the target magnetospheric SWCX emission and seven background components: astronomical point sources, soft proton flares, particle background, cosmic background (constant), residual instrumental lines (not in the 0.5–0.7 keV band), residual soft proton contamination (not highly variable in an observation), and heliospheric SWCX emissions (relatively stable on half-day timescales). For this study, it is sufficient to remove signals from astronomical point sources, soft proton flares, and the particle background.

First, we created a region filter using the list of astrophysical point sources available in the XMM-Newton Science Archives, which removed events within an appropriate radius (primarily within $35''$) centered on each source. Here we manually observed each event file to check for residual point, diffuse, or extended astronomical sources. Second, to clean up the soft proton flares, we used the SAS task espfilt, which fitted a rough Gaussian to the histogram of the light-curve values and created good time intervals for the count rates in the range of 2.5σ around this Gaussian peak. Third, we used the SAS task evqpb

⁷ <http://nxsas.esac.esa.int/nxsas-web/>

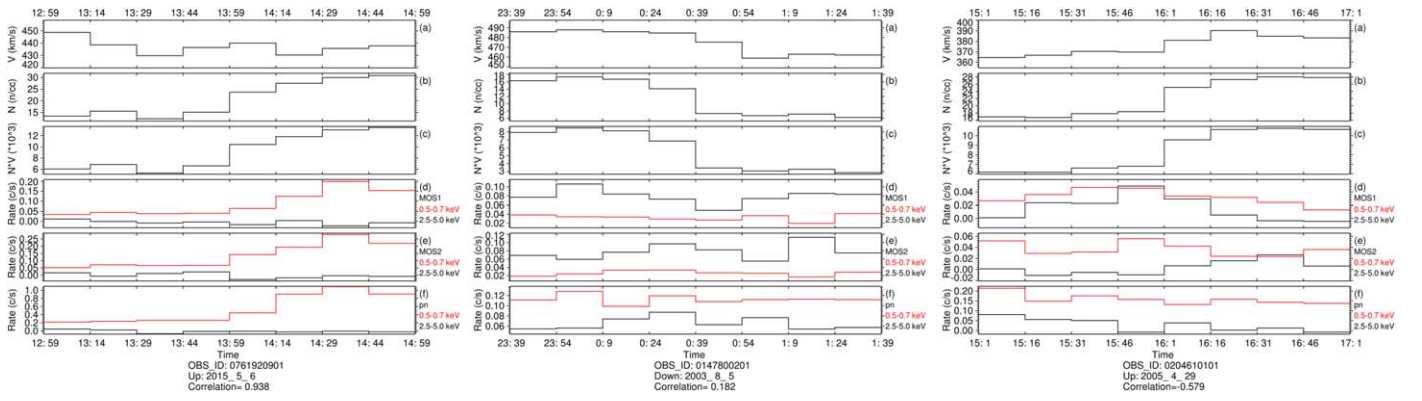


Figure 3. Correlations for three cases, from left to right: positive correlation, uncorrelated, and negative correlation. Solar wind conditions: (a) velocity, (b) proton density, and (c) proton flux. Also shown is the count rate of XMM-Newton in the 0.5–0.7 keV (red) and 2.5–5.0 keV (black) bands from (d) MOS1, (e) MOS2, and (f) pn after removing the first three backgrounds.

to create a list of particle background events from the filter wheel closed set and then derived the scaling factor by comparing the products extracted from this particle background event list with the products extracted from the original event list. Here, to avoid the influence of signals other than the particle background, the energy band of 2.5–12.0 keV was used for the MOS, and the same energy band excluding 7.2–10 keV was used for the pn. After removing the first three backgrounds, we finally obtained a soft X-ray signal consisting of the target time-varying magnetospheric SWCX emission and last four stable backgrounds (Carter et al. 2010; Zhang et al. 2022).

2.3. Calculating Each Case’s Linear Correlation Coefficient

This paper uses the 15 minute averaged XMM-Newton count rate and OMNI 1 minute solar wind data for 1 hr before and after the sudden change in proton flux (2 hr in total). The choice of 15 minutes rather than a shorter time resolution was to reduce count rate errors due to the narrow FOV of XMM-Newton. The selection of 2 hr rather than a more extended analysis duration further reduced the influence of other factors, as they were relatively stable on this timescale.

For each case, there were three linear correlation coefficients between the XMM-Newton count rate and the solar wind proton flux because XMM-Newton had three cameras. We adopted the average of the three correlation coefficients as each case’s final correlation coefficient (r). We defined a significant correlation to be $|r| \geq 0.8$, a strong correlation to be $0.5 \leq |r| < 0.8$, a weak correlation to be $0.3 \leq |r| < 0.5$, and a nonexistent correlation to be $|r| < 0.3$. Figure 3 shows the correlations of three cases: positive correlation ($r \geq 0.3$), uncorrelated ($-0.3 < r < 0.3$), and negative correlation ($r \leq -0.3$). The comparison of the count rate in the 0.5–0.7 keV band and that in the 2.5–5.0 keV band demonstrates that this change is due to the SWCX emission.

Table 1 shows the details of 100 selected XMM-Newton cases. In all cases, the LOS does not pass through the space-confined helium-focusing cone with strong heliospheric SWCX emission, which is conducive to improving the signal-to-noise ratio of magnetospheric SWCX emission. Note that when the LOS is along the solar wind Parker spiral, the heliospheric SWCX emission might become important and would be correlated with the magnetospheric SWCX emission. However, this situation accounts for a very small proportion, so it will not have a disruptive effect on the statistical results (Snowden et al. 2004; Koutroumpa et al. 2006, 2007, 2009; Kuntz et al. 2015).

3. Results

3.1. Different Parameters of the Solar Wind Proton Flux

Figure 4 shows the relationship between the linear correlation coefficients and four solar wind proton flux parameters: proton flux (NV), proton flux change value (ΔNV), proton density (N), and velocity (V). The middle and top panels of each graph show the absolute value of the linear correlation coefficient, which corresponds to the degree of correlation. They also show the percentage of cases within a given range of correlation coefficient, which corresponds to the probability of that correlation. First, the degree of correlation increases distinctly with NV , ΔNV , and N and reaches a strong positive correlation when $NV > 10,000$ n*km/cc/s, $\Delta NV > 6000$ n*km/cc/s, or $N > 20$ n/cc (number/cubic centimeter). Second, the probability of a positive correlation increases significantly with NV , ΔNV , and N and becomes greater than 50% when $NV > 10,000$ n*km/cc/s, $\Delta NV > 6000$ n*km/cc/s, or $N > 30$ n/cc. Third, the effect of velocity is not obvious; the degree and probability of a positive correlation seem to reach a maximum when $400 \text{ km s}^{-1} < V < 500 \text{ km s}^{-1}$ and $300 \text{ km s}^{-1} < V < 400 \text{ km s}^{-1}$, respectively.

To sum up, there is a dynamical response of the magnetospheric SWCX emission intensity to the solar wind proton flux. This dynamical response is weak when the solar wind proton flux is low ($< 10,000$ n*km/cc/s) because the variation of the SWCX signal is smaller than the uncertainty due to counting statistics for the other emission components. However, this dynamical response increases with the solar wind proton flux and its change value. Instrumental simulations by Guo et al. (2022) revealed that the large-scale magnetopause could be well reconstructed when $N \geq 12 \text{ cm}^{-3}$, which is slightly smaller than this observation, probably due to the instrumental simulations using a simplified fixed cosmic background. In addition, the nonsignificant existence of negative correlation cases is predictable due to some inevitable issues mentioned above, such as the relative location of the LOS and the magnetopause.

3.2. Valence State of Solar Wind Ions

We characterized the valence state of the solar wind ions by using the 2 hr data from the Advanced Composition Explorer (ACE)⁸: the ratio of O^{7+} to O^{6+} ($\text{O}^{7+}/\text{O}^{6+}$). The reasons are (1) SWCX emission in the 0.5–0.7 keV band is dominated by

⁸ <https://cdaweb.gsfc.nasa.gov/index.html>

Table 1
Details of 100 Selected XMM-Newton Cases

ObsID (1)	Date (2)	Time (3)	Type (4)	Correlation (5)	ObsID (6)	Date (7)	Time (8)	Type (9)	Correlation (10)
0092850201 ^a	2001/4/28	23:57	Up	0.5964	0654880301	2011/3/30	0:41	Down	0.5581
0111550101	2001/5/18	13:50	Down	-0.4936	0654880201	2011/4/11	17:17	Down	0.2634
0100440101 ^a	2001/5/28	12:06	Down	-0.368	0690500101	2013/2/5	4:37	Down	-0.3032
0100440101 ^a	2001/5/28	19:48	Down	0.316	0692840501	2013/2/12	16:16	Down	-0.2321
0111550401	2001/6/1	18:27	Up	0.4411	0692840501	2013/2/12	21:51	Down	0.1968
0111550401	2001/6/1	22:43	Down	0.5826	0692840501	2013/2/13	13:12	Down	0.2388
0112880201 ^a	2001/7/9	10:22	Down	0.0017	0690680201	2013/3/20	23:06	Down	0.1427
0109490101	2001/9/5	19:24	Down	-0.0496	0693190401	2013/3/27	12:42	Down	-0.1099
0109490601	2001/9/10	4:43	Down	-0.003	0695200301	2013/4/14	9:15	Up	-0.2842
0094400101	2001/9/11	18:17	Down	0.4788	0728980201	2013/11/5	10:05	Up	0.5427
0022740201 ^a	2001/10/27	21:31	Up	0.3744	0722360301	2013/11/27	12:59	Up	0.1808
0134540601	2002/8/23	4:06	Up	0.0706	0723450201	2014/1/11	22:49	Up	-0.2682
0147540101	2002/10/30	2:29	Down	0.7221	0720173501	2014/3/30	21:37	Down	0.0879
0150320201 ^a	2003/6/17	19:46	Down	-0.4325	0720173701	2014/4/10	9:02	Down	0.0471
0148450701	2003/7/6	15:57	Down	-0.1019	0720173901	2014/4/14	0:48	Up	0.5239
0153450101	2003/7/9	19:01	Up	-0.1466	0748391101 ^a	2015/1/7	11:38	Down	0.8759
0145800101	2003/7/14	11:20	Up	0.6193	0761920901 ^a	2015/5/6	13:59	Up	0.9383
0141751201	2003/7/26	0:56	Down	-0.2013	0761630101	2016/1/5	17:48	Down	0.1651
0147800201	2003/8/4	18:08	Up	0.3501	0761630101	2016/1/5	23:19	Up	-0.0178
0147800201	2003/8/4	22:24	Up	-0.0724	0761630101	2016/1/6	1:47	Down	-0.024
0147800201	2003/8/5	0:39	Down	0.1818	0761630101	2016/1/6	14:41	Up	0.2778
0200270101	2004/6/25	13:19	Down	-0.1814	0760750101	2016/2/2	21:47	Down	0.0378
0200370101	2004/8/16	2:16	Up	-0.2265	0763720301	2016/3/22	7:44	Up	0.3455
0203541101	2004/8/18	13:35	Up	0.5078	0784370301	2016/10/22	23:13	Down	0.0353
0164560901	2004/9/12	21:21	Down	0.0569	0780090801	2016/10/25	8:12	Up	-0.031
0204610101	2005/4/29	16:01	Up	-0.5792	0803050801	2017/4/9	2:25	Up	0.0701
0305920601	2005/6/23	10:05	Down	0.8527	0800630101	2017/12/19	22:45	Up	0.116
0212480801	2005/7/1	15:32	Down	0.8866	0802220401	2018/1/31	11:43	Down	-0.3803
0311190101	2006/5/3	21:06	Down	-0.3863	0800271101	2018/2/26	13:32	Down	0.1894
0302351801	2006/5/17	20:24	Up	0.2957	0824910201	2018/10/26	20:36	Down	-0.0898
0506440101	2007/5/31	23:28	Down	0.0867	0824910201	2018/10/26	21:14	Up	0.2543
0504100901	2007/6/21	7:19	Up	0.0377	0830440101	2019/1/10	23:41	Up	0.5784
0555460201	2008/5/11	2:57	Down	-0.0254	0827211501	2019/1/13	11:08	Up	-0.092
0556230201	2008/6/10	13:55	Up	0.2886	0831790701	2019/1/17	6:18	Down	0.1151
0550452601	2008/12/14	4:28	Down	-0.0514	0831790701	2019/1/17	13:00	Down	-0.3728
0553030101	2008/12/18	17:46	Down	-0.2444	0820720101	2019/2/20	15:17	Up	0.4052
0560181101	2009/2/3	20:30	Up	0.3509	0827201101	2019/2/25	6:27	Down	0.3016
0560181101	2009/2/3	23:14	Up	0.179	0842592201	2019/9/17	8:21	Up	0.1547
0554740801	2009/3/12	17:44	Up	0.304	0841920101	2019/10/21	4:44	Down	0.3481
0600450101	2009/6/24	15:42	Up	0.2527	0844860401	2020/1/2	23:12	Up	-0.0828
0602920101	2009/7/10	4:50	Down	-0.2823	0844860401	2020/1/3	8:05	Down	0.1063
0604060101	2009/12/30	0:07	Up	-0.0999	0844860701	2020/1/8	15:22	Down	0.0749
0604961801	2010/2/17	20:35	Up	0.0591	0844860701	2020/1/9	9:34	Down	0.0659
0604980201	2010/3/1	16:36	Up	0.0203	0844860701	2020/1/9	16:09	Down	0.2182
0603741101	2010/3/24	14:15	Up	0.3277	0864330101	2020/1/11	11:56	Up	0.0276
0602520401	2010/3/25	17:47	Down	0.0349	0870920101	2020/9/13	20:30	Up	0.3237
0652401401	2010/12/30	2:58	Up	-0.1264	0870920101	2020/9/14	1:36	Down	0.1572
0650560601	2011/2/4	2:45	Up	-0.1612	0870920101	2020/9/14	9:14	Up	-0.0262
0655300301	2011/2/4	10:33	Down	0.1772	0827060601	2020/10/5	14:59	Up	-0.2162
0655610101	2011/2/18	8:23	Down	0.2402	0870820101	2020/10/19	20:40	Down	-0.4337

Note. We list the observation identifier, date, time, type of sudden change in the solar wind proton flux, and linear correlation coefficient.

^a During an ICME.

oxygen ions, and (2) it is one of the most commonly used ion parameters to determine the interplanetary coronal mass ejection (ICME; Richardson & Cane 2004; Zurbuchen & Richardson 2006; Richardson & Cane 2010; Richardson 2014). Here we took into account the travel time of the solar wind

from the ACE to Earth, which averaged around 1 hr. On the one hand, the ACE data before and after 2011 August 23 are discontinuous, so they cannot be confused. On the other hand, there are only two cases of solar wind proton flux greater than 10,000 n*km/cc/s in the data set after 2011 August 23, so

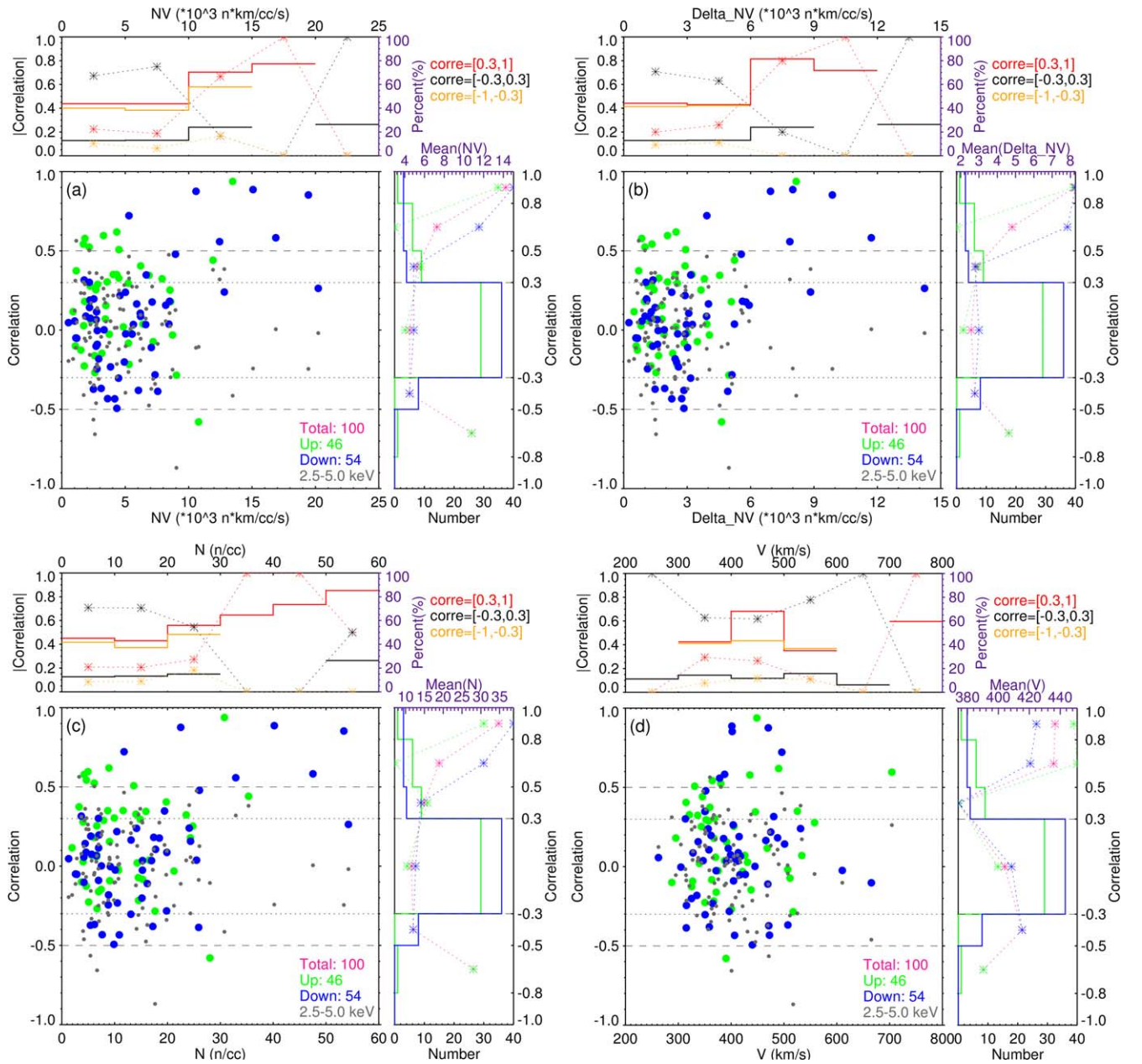


Figure 4. Relationship between linear correlation coefficients and four solar wind parameters (maximum value in each observation): (a) proton flux, (b) proton flux change value, (c) proton density, and (d) velocity. The histogram in the top panel of each graph represents the absolute value of the linear correlation coefficient, and the asterisk curve represents the percentage of cases within a given range of correlation coefficients. The histogram in the right panel of each graph represents the number of cases, and the asterisk curve represents the average solar wind conditions for each bin of the correlation coefficient. Red, black, and orange represent positive, uncorrelated, and negative correlations. Green and blue represent sudden increases and decreases in the solar wind proton flux. Pink represents the sum of all cases. The correlation coefficient of the 2.5–5.0 keV band is in gray.

valid statistical results cannot be obtained from this data set. Therefore, we finally analyzed the data set consisting of 52 cases using the ACE data before 2011 August 23.

First of all, we independently studied the effect of the solar wind ion valence state on the correlation. As shown in panel (a) of Figure 5, the probability of correlation has a trend of increasing with the increasing valence state of the solar wind ions, while the degree of correlation seems to be insensitive to the valence state of the solar wind ions. Since the intensity of SWCX emission is determined by the solar wind proton flux and the solar wind ion abundance, we took the product of the solar wind proton flux and the ratio of O^{7+} to O^{6+} as a parameter. As shown in panel (b) of Figure 5, the probability

and degree of correlation both increase with the product. In addition, we also studied the joint effect of the solar wind proton flux and ion valence state. As shown in panel (c) of Figure 5, although the proton flux is relatively low, the correlation may exist when the ion valence state is high. Moreover, the valence state of the solar wind ions is not correlated with the solar wind proton flux but is anticorrelated during the ICME. There are eight cases during an ICME, which are identified by the list compiled by Ian Richardson and Hilary Cane.⁹ The ion valence states of all ICME cases are quite high,

⁹ <https://izw1.caltech.edu/ACE/ASC/DATA/level3/icmetable2.htm>

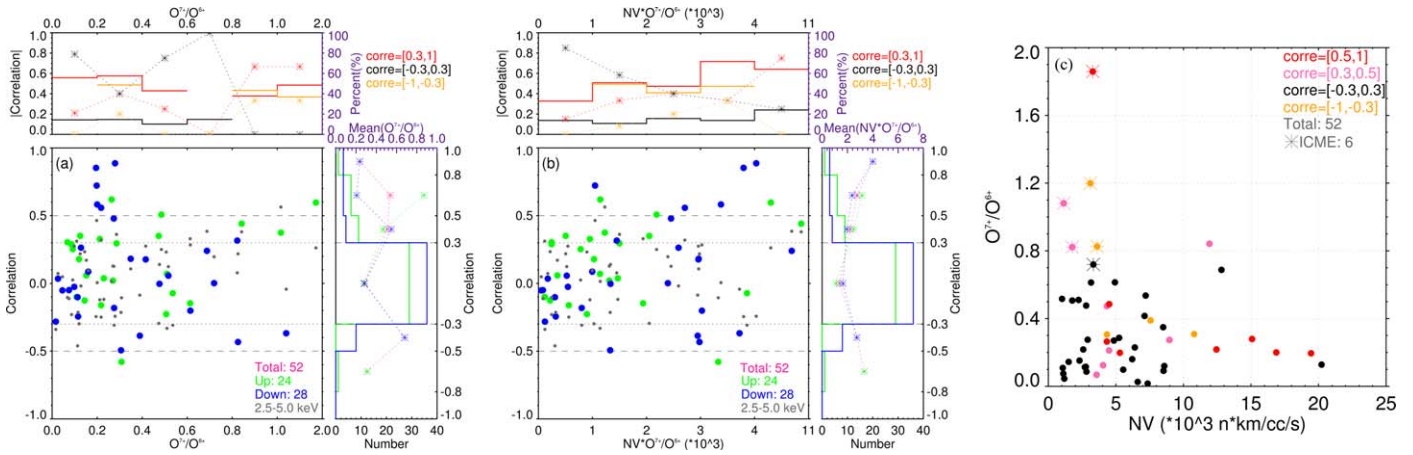


Figure 5. Relationship between linear correlation coefficients and two parameters: (a) the ratio of O^{7+} to O^{6+} and (b) the product of the solar wind proton flux and the ratio of O^{7+} to O^{6+} . The descriptions of panels (a) and (b) are the same as in Figure 4. The asterisks in panel (c) indicate the cases during an ICME.

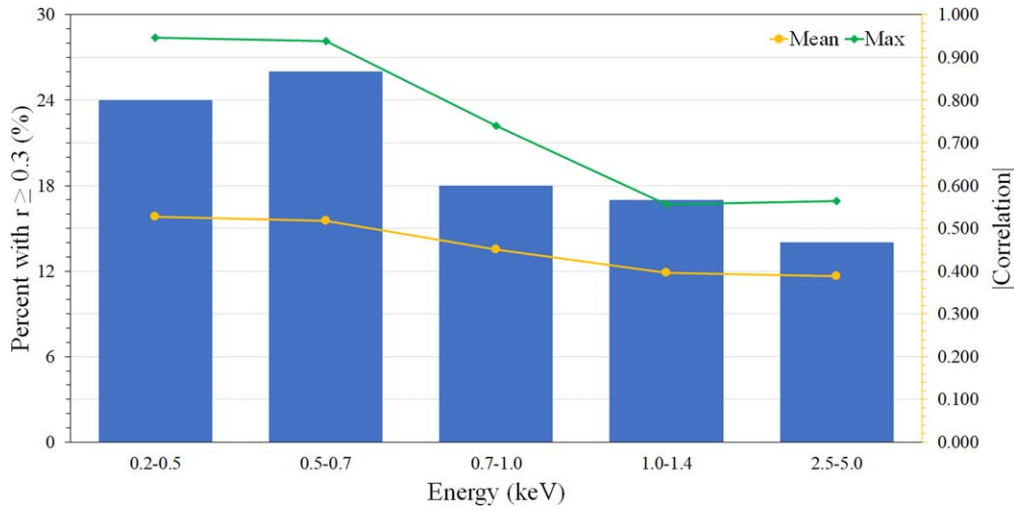


Figure 6. Relationship between positive correlation coefficients ($r \geq 0.3$) and different energy bands. The histogram represents the percentage of correlation. The curves represent the absolute value of the linear correlation coefficient, where yellow and green represent the mean and maximum values.

and the probability of strongly correlated:weakly correlated:uncorrelated for the ICME is 37.5%:50%:12.5%, while that for no ICME is 14%:21%:65%. This is because the abundance of solar wind ions that can generate SWCX emission in the ICME has increased. The probability of negative correlation for the ICME is 25%, while that for no ICME is 9%. This may be caused by the inconsistent change of the solar wind proton flux and ion valence state, as the proton flux in the ICME will decrease due to expansion, but the ion valence state will increase, as its source is the active region on the Sun, which is also the reason for the anticorrelation between the proton flux and ion valence state in the ICME.

To sum up, the importance of the solar wind ion valence state is much less than that of the proton flux, as the solar wind ion valence state mainly plays a regulation role in the dynamical response of the magnetospheric SWCX emission intensity to the solar wind proton flux. The probability of this correlation increases with the solar wind ion valence state because there are more ions to generate SWCX emission. The dynamical response may exist if the valence state of the solar wind ions is high, even when the proton flux is relatively low. In addition, for the ICME, the probability and degree of this correlation increased distinctly, which is conducive to the study

of ICMEs because the solar wind ions in ICMEs are usually highly ionized (Richardson & Cane 2010; Richardson 2014).

3.3. SWCX Emission in Different Energy Bands

Figure 6 shows the positive correlation ($r \geq 0.3$) of the magnetospheric SWCX emission in different energy bands. The probability of correlation is highest in the 0.5–0.7 keV band, followed by the 0.2–0.5 keV band, and then decreases with increasing energy. The degree of correlation is close to the 0.2–0.5 and 0.5–0.7 keV bands and then decreases with increasing energy. In general, for XMM-Newton, the correlation is strongest in the 0.5–0.7 keV band, followed by the 0.2–0.5 keV band, and then becomes weaker with increasing energy. It is somewhat different from the results of Kuntz et al. (2015) based on ROSAT data. The 0.2–0.5 keV band in XMM-Newton is very different from the ROSAT 1/4 keV band. (1) The response of XMM-Newton drops rapidly in this band and has no good characteristics below 0.3–0.4 keV, so there are not as many SWCX counts. (2) The low-energy “electronic noise” makes a great contribution to this band. Thus, many counts are not due to the actual emission of this band. (3) The particle background is not well characterized in this band, but it is clear that it is increasing rapidly to lower energies. Therefore, the

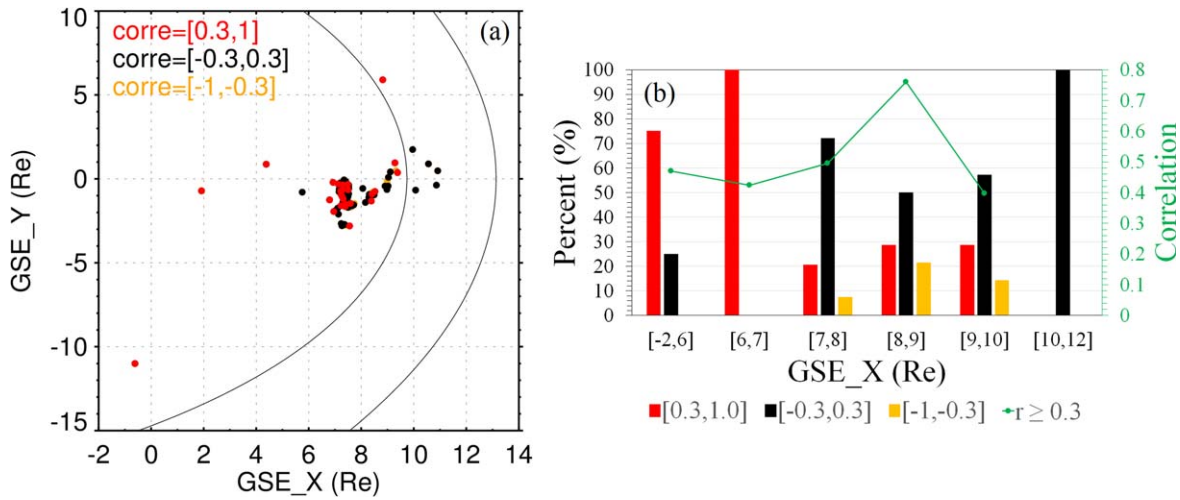


Figure 7. Relationship between linear correlation coefficients and the position of XMM-Newton in GSE coordinates. The locations of the magnetopause and bow shock in panel (a) are calculated using the average solar wind conditions of all 100 cases. In panel (b), the bars represent the percentage of cases within a given range, and the green line indicates the value of the positive correlation coefficient ($r \geq 0.3$).

ratio of SWCX counts to all other components is likely to be much lower in this band than in the 0.5–0.7 keV band, which will reduce the amount of correlation. For the 0.5–0.7 keV band, because it contains little more than the ROSAT 3/4 keV band, especially in terms of SWCX emission, it is questionable whether our correlation coefficient is comparable to that of Kuntz et al. (2015). For the higher-energy band, the correlation becomes weaker because the SWCX emission decreases at higher energy.

3.4. Position of XMM-Newton

Figure 7 shows the relationship between the linear correlation coefficients and the position of XMM-Newton in geocentric solar ecliptic (GSE) coordinates. Since the XMM-Newton orbit is highly inclined ($\sim 70^\circ$), all of the points shown in the left panel are near or below the magnetopause in the GSE-Z direction. Note that XMM-Newton observes (roughly) perpendicular to the GSE-X axis. For $\text{GSE-X} < 7$ Re, the probability of a positive correlation is very high, but the degree is not very high. This is because XMM-Newton is within (or close to) the magnetopause. Thus, no matter what direction it is looking, it is looking through the bulk of the magnetosheath, though not with a very long path length. Thus, the bulk of the observations are correlated, though the degree of correlation may be weak. On the contrary, for $\text{GSE-X} < 10$ Re, the probability of a positive correlation is very low. This is because XMM-Newton is outside the magnetopause and possibly outside the bow shock. Whether or not it sees the magnetosheath depends upon the look direction. If it is looking through a long path length, it will get a very strong correlation, but there are lots of directions in which one can look and see almost nothing of the magnetosheath. For $7 \text{ Re} < \text{GSE-X} < 10$ Re, the probability and degree of positive correlation are highest at 8–9 Re. In general, when XMM-Newton locates downstream of the magnetopause and is closer to the subsolar magnetopause, the probability and degree of correlation are higher. On the one hand, the SWCX emissivity near the subsolar magnetopause is the strongest. On the other hand, when XMM-Newton observes from the inside magnetosphere to the outside, its integral path in the magnetosheath is the longest.

4. Discussion

4.1. Inconsistent Changes in Solar Wind Ion Flux and Proton Flux

The intensity of SWCX emission is actually determined by the flux of high-valence solar wind ions, but most studies focus on proton flux rather than ion flux. The reasons are as follows. (1) Solar wind ion data are scarce and have a low signal-to-noise ratio and time resolution. (2) There are many kinds of solar wind ions, and the changes of each ion are not completely consistent, so it is difficult to characterize them perfectly with a simple parameter. (3) Since the location of the magnetopause is strongly correlated with the solar wind flux, and the SWCX emissivity is very strongly correlated with the location of the magnetopause, the proton flux should be responsible for the bulk of the variation of the SWCX emission. (4) By the time the solar wind reaches the Earth, the ion fractions are frozen in (Lepri et al. 2013). Thus, the ion density tends to track the proton density over relatively short periods of time. However, the inconsistent change in solar wind ion flux and proton flux can occur when changes in the valence state of ions are opposite and more intense than changes in proton flux. The ICME is a typical example. Since the proton flux in an ICME is reduced by expansion, while the ions have a higher valence state, there may be a positive or negative correlation between the magnetospheric SWCX emission intensity and the solar wind proton flux.

4.2. Differences between the Increase and Decrease in Solar Wind Proton Flux






As shown in the middle and right panels of Figure 4, although the solar wind proton flux is weaker, the correlation is slightly better when the proton flux suddenly increases rather than decreases. As shown in the middle and right panels of Figure 5(a), the valence state of solar wind ions is slightly higher when the proton flux suddenly increases rather than decreases, which adds a favorable factor to the magnetospheric SWCX emission intensity, further leading to a stronger correlation. It may be because the sudden increases in the solar wind proton flux are often associated with explosive activity on the Sun, such as flares and ICMEs.

5. Conclusions

This work studies the dynamic response of SWCX soft X-ray emission in the Earth's magnetosphere to the solar wind proton flux. Unlike previous studies that attempted to use complex MHD models to match the details of observed SWCX of a necessarily limited number of cases, this work focuses on determining the changes over individual observations in a much larger sample. To provide the cleanest test, we selected 100 XMM-Newton cases observed when the solar wind proton flux changed suddenly by a factor greater than 1.5 and calculated the correlation coefficient between the solar wind proton flux and the count rate in the 0.5–0.7 keV band containing the O VII and O VIII SWCX lines. We find that the dynamical response is weak when the solar wind proton flux is low ($<10,000 \text{ n}^* \text{ km/cc/s}$) because its variation is smaller than the uncertainty due to other emission components, but this response increases with the proton flux and its change value. The dynamical response is improved when the valence state of the solar wind ions is high, as a higher abundance of ions generating the SWCX emission can produce a greater correlation even when the proton flux is relatively low. It is conducive to the study of ICMEs because the solar wind ions in ICMEs are usually highly ionized. For XMM-Newton, the 0.5–0.7 keV band shows the strongest correlation, as the instrumental response decreases at lower energies and the SWCX emission decreases at higher energies. Moreover, the closer the satellite LOS is to the subsolar magnetopause with the strongest SWCX emissivity, the better the correlation.

This work was supported by NNSFC grants 42188101 and 42074202; the Strategic Pioneer Program on Space Science, CAS grant No. XDA15350201; and in part by the Research Fund from the Chinese Academy of Sciences and the Specialized Research Fund for State Key Laboratories of China. T.S. is also supported by the Young Elite Scientists Sponsorship Program (CAST—Y202045). J.A.C. is supported by Royal Society grant DHF\R1\211068. D.K. is supported by CNES through the “Soleil Héliosphère Magnétosphère” program.

ORCID iDs

Yingjie Zhang  <https://orcid.org/0000-0003-4777-9552>
 Tianran Sun  <https://orcid.org/0000-0002-3042-247X>
 Jennifer A. Carter  <https://orcid.org/0000-0002-0981-2895>
 Steve Sembay  <https://orcid.org/0000-0002-3700-9784>
 Dimitra Koutroumpa  <https://orcid.org/0000-0002-5716-3412>
 Li Ji  <https://orcid.org/0000-0001-7500-0660>
 Wenhao Liu  <https://orcid.org/0000-0002-0924-9668>

Chi Wang  <https://orcid.org/0000-0001-6991-9398>

References

- Asakura, K., Matsumoto, H., Okazaki, K., et al. 2021, *PASJ*, **73**, 504
 Branduardi-Raymont, G., Elsner, R. F., Gladstone, G. R., et al. 2004, *A&A*, **424**, 331
 Branduardi-Raymont, G., Sembay, S. F., Eastwood, J. P., et al. 2012, *ExA*, **33**, 403
 Branduardi-Raymont, G., Wang, C., Escoubet, C. P., et al. 2018, SMILE definition study report, European Space Agency, ESA/SCI, 1, 2018
 Carter, J., Sembay, S., & Read, A. 2012, *AN*, **333**, 313
 Carter, J. A., & Sembay, S. 2008, *A&A*, **489**, 837
 Carter, J. A., Sembay, S., & Read, A. M. 2010, *MNRAS*, **402**, 867
 Carter, J. A., Sembay, S., & Read, A. M. 2011, *A&A*, **527**, A115
 Chao, J., Wu, D., Lin, C., et al. 2002, in Proc. COSPAR Coll. 12, Space Weather Study Using Multipoint Techniques, ed. L.-H. Lyu (Oxford: Pergamon), 127
 Collier, M., Porter, F., Sibeck, D., et al. 2012, *AN*, **333**, 378
 Collier, M. R., Snowden, S. L., Sarantos, M., et al. 2014, *JGRE*, **119**, 1459
 Cravens, T. E. 1997, *GeoRL*, **24**, 105
 Cravens, T. E. 2000, *ApJL*, **532**, L153
 Dennerl, K., Lisse, C. M., Bhardwaj, A., et al. 2006, *A&A*, **451**, 709
 Ezo, Y., Ebisawa, K., Yamasaki, N. Y., et al. 2010, *PASJ*, **62**, 981
 Ezo, Y., Miyoshi, Y., Yoshitake, H., et al. 2011, *PASJ*, **63**, S691
 Fujimoto, R., Mitsuda, K., McCammon, D., et al. 2007, *PTPS*, **169**, 71
 Guo, Y., Sun, T., Wang, C., & Sembay, S. 2022, *ScChD*, **65**, 1601
 Henley, D. B., & Shelton, R. L. 2010, *ApJS*, **187**, 388
 Henley, D. B., & Shelton, R. L. 2012, *ApJS*, **202**, 14
 Ishi, D., Ishikawa, K., Miyoshi, Y., Terada, N., & Ezo, Y. 2022, *PASJ*, **75**, 128
 Ishi, D., Ishikawa, K., Numazawa, M., et al. 2019, *PASJ*, **71**, 23
 Ishikawa, K., Ezo, Y., Miyoshi, Y., et al. 2013, *PASJ*, **65**, 63
 Koutroumpa, D., Acero, F., Lallement, R., Ballet, J., & Kharchenko, V. 2007, *A&A*, **475**, 901
 Koutroumpa, D., Collier, M. R., Kuntz, K. D., Lallement, R., & Snowden, S. L. 2009, *ApJ*, **697**, 1214
 Koutroumpa, D., Lallement, R., Kharchenko, V., et al. 2006, *A&A*, **460**, 289
 Kuntz, K. D. 2018, *A&ARv*, **27**, 1
 Kuntz, K. D., Collado-Vega, Y. M., Collier, M. R., et al. 2015, *ApJ*, **808**, 143
 Kuntz, K. D., & Snowden, S. L. 2008, *ApJ*, **674**, 209
 Lepri, S. T., Landi, E., & Zurbuchen, T. H. 2013, *ApJ*, **768**, 94
 Lisse, C. M., Dennerl, K., Englhauser, J., et al. 1996, *Sci*, **274**, 205
 Richardson, I. G. 2014, *SoPh*, **289**, 3843
 Richardson, I. G., & Cane, H. V. 2004, *JGRA*, **109**, A09104
 Richardson, I. G., & Cane, H. V. 2010, *SoPh*, **264**, 189
 Shue, J.-H., Chao, J. K., Fu, H. C., et al. 1997, *JGR*, **102**, 9497
 Sibeck, D. G., Allen, R., Aryan, H., et al. 2018, *SSRv*, **214**, 79
 Snowden, S. L., Collier, M. R., & Kuntz, K. D. 2004, *ApJ*, **610**, 1182
 Snowden, S. L., Egger, R., Freyberg, M. J., et al. 1997, *ApJ*, **485**, 125
 Sun, T., Wang, X., & Wang, C. 2021, *JGRA*, **126**, e2020JA028314
 Sun, T. R., Wang, C., Sembay, S. F., et al. 2019, *JGRA*, **124**, 2435
 Sun, T. R., Wang, C., Wei, F., & Sembay, S. 2015, *JGRA*, **120**, 266
 Wang, C., & Branduardi-Raymont, G. 2020, *ChJSS*, **40**, 700
 Wargelin, B. J., Markevitch, M., Juda, M., et al. 2004, *ApJ*, **607**, 596
 Whittaker, I. C., Sembay, S., Carter, J. A., et al. 2016, *JGRA*, **121**, 4158
 Zhang, Y., Sun, T., Wang, C., et al. 2022, *ApJL*, **932**, L1
 Zurbuchen, T. H., & Richardson, I. G. 2006, *SSRv*, **123**, 31